

01,11

Structures and phase transitions in Fe-Ga-Al alloys

© A.M. Balagurov^{1,2,3}, I.A. Bobrikov^{1,2}, S.V. Sumnikov^{1,2}, B. Yerzhanov⁴, D.G. Chubov²,
V.V. Palacheva², I.S. Golovin^{2,5}

¹ Joint Institute for Nuclear Research,
Dubna, Moscow oblast, Russia

² National University of Science and Technology MISiS,
Moscow, Russia

³ Lomonosov Moscow State University,
Moscow, Russia

⁴ Kazan Federal University,
Kazan, Russia

⁵ Moscow Polytechnic University,
Moscow, Russia

E-mail: bobrikov@nf.jinr.ru, bekarys@mail.ru

Received July 18, 2022

Revised July 18, 2022

Accepted July 19, 2022

Evolution of structural phases and microstructural cast state of $\text{Fe}_{100-(x+y)}\text{Ga}_x\text{Al}_y$ compositions in the range of $17 \leq (x + y) \leq 39$ at.% was studied in neutron diffraction experiments performed with high resolution and in continuous temperature scanning mode when heated to $\sim 900^\circ\text{C}$ and subsequent cooling. It is established that the structures of the cast states of triple alloys in the studied range of Ga and Al content basically repeat the structure of the double compositions $\text{Fe}_{100-x}\text{Ga}_x$ up to $x \approx 30$ and $\text{Fe}_{100-y}\text{Al}_y$ up to $y \approx 50$. Namely, only cubic phases (A2, D0₃ and B2) are observed in them, and hexagonal (A3, D0₁₉) and monoclinic (such as $\text{Fe}_{13}\text{Ga}_9$ or $\alpha\text{-Fe}_6\text{Ga}_5$) there are no phases characteristic of the Fe-Ga system. The expansion of the range of formation of cubic phases formed on the basis of the BCC cell in ternary alloys in comparison with $\text{Fe}_{100-x}\text{Ga}_x$ indicates the role of Al in the stabilization of these structures.

Keywords: alloys Fe-Ga, Fe-Al, Fe-Ga-Al, structural phase transitions, neutron diffraction, magnetostriction.

DOI: 10.21883/PSS.2022.12.54375.444

1. Introduction

The discovery of a significant increase in the magnetostriction of $\alpha\text{-Fe}$ with partial substitution of iron for gallium caused the appearance of a large number of studies in which a similar effect was sought in a variety of binary (Fe-Al, Fe-Ge, Fe-Si, etc.) and triple (Fe-Ga-Al, Fe-Ga-Ge, etc.) iron-based alloys. In one of the first review papers on this topic [1], a comparison of the behavior of the tetragonal magnetostriction constant $(3/2)\lambda_{100}$ is given for $\text{Fe}_{100-x}\text{Ga}_x$ and $\text{Fe}_{100-x}\text{Al}_x$ alloys and the influence of third elements on it (Ni, Co, Sn, Si, Ge and etc.). It turned out that any options for replacing gallium with other elements or additives to the Fe-Ga alloy of any third elements (with the exception of rare earths) reduce the magnetostriction constant to one degree or another. A somewhat more detailed analysis of the effects of gallium substitution in the Fe-Ga alloy was carried out in [2], where the experimental values are given $(3/2)\lambda_{100}$ for binary Fe-Ga, Fe-Al, Fe-Ge, Fe-Si and triple Fe-Ga-Al, Fe-Ga-Ge-alloys in the range of iron substitution up to 35%. In both papers ([1] and [2]), magnetostriction data are given for single crystals in two states: after quenching in water and after relatively slow cooling in a furnace. In hardened samples, magnetostriction turned out to be slightly higher

(by $\sim 20\%$), but its dependence on the content of the alloying element is generally the same for both states. For Fe-Ga, the data of both papers correspond well to each other, confirming, in particular, the presence of two maxima at $x \approx (17-20)$ at.% and $(26-29)$ at.%. For Fe-Al, the maximum is one, somewhat more clearly expressed in the data given in [2], according to which the maximum values of magnetostriction are reached at $x \approx (16-19)$ at.%. At maximum, they make up about 60% noticeably more than when replacing Ga with other elements.

A relatively small deterioration in magnetostrictive properties in Fe-Al alloys allows us to consider them as a worthy replacement for more expensive and not very good mechanical properties (excessive brittleness) Fe-Ga alloys. An important factor is also the similarity of the crystal and electronic structures of Fe-Ga and Fe-Al alloys. From this point of view, triple alloys Fe-Ga-Al are even more promising. From the data given in [2], it follows that for the alloy $\text{Fe}_{83.0}\text{Ga}_{8.5}\text{Al}_{8.5}$ constant $(3/2)\lambda_{100}$ has a maximum value of ~ 250 ppm, which is about 70% of the magnetostriction level in Fe-Ga and noticeably exceeds its maximum values in Fe-Ge, Fe-Si and Fe-Ga-Ge-alloys.

To compare the characteristics of alloys consisting of different elements, the authors of [2] use the ratio of the

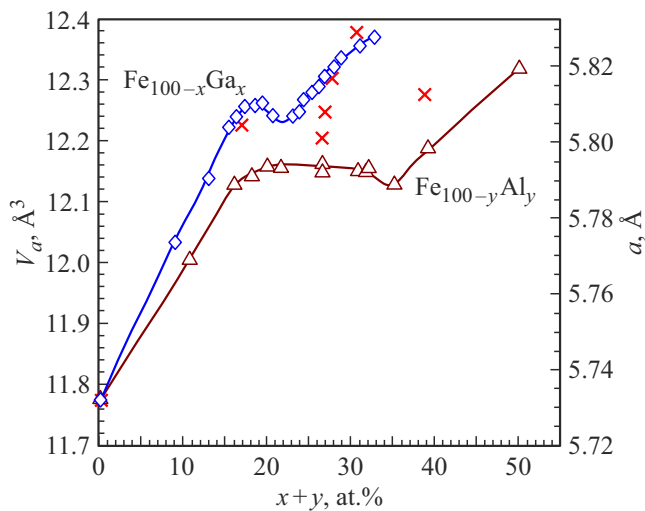


Figure 1. Atomic volume (left scale) for the compositions $\text{Fe}_{100-x}\text{Ga}_x$ (rhombuses), $\text{Fe}_{100-y}\text{Al}_y$ (triangles) and $\text{Fe}_{100-(x+y)}\text{Ga}_x\text{Al}_y$ (crosses) as a function of the variable $(x+y)$. The lines are drawn for ease of perception. Right scale — cell parameter values for phase D0_3 . Dot errors are smaller than the character size.

number of free electrons to the number of atoms (electron-to-atom ratio), e/n . However, for Ga and Al, the number of free electrons is assumed to be the same, namely, $e = 3$ (for iron $e = 1$), therefore, for the alloy $\text{Fe}_{100-(x+y)}\text{Ga}_x\text{Al}_y$ values e/n and $(x+y)$ are related by the linear relation $[e/n = 1 + 0.02(x+y)]$ and can be used equally. As an example, Fig. 1 shows the atomic volumes (cell volume per atom) of binary and ternary compositions as functions of the total content of Ga and Al, constructed from neutron diffraction data obtained in [3] and in this paper. The characteristic S-shaped shape of the dependencies is associated with the ordering effects in alloys, namely, with the formation of the structural phases D0_3 and B2. It can be seen that the value of the atomic volume for a triple alloy generally corresponds to the trend of its change for double alloys.

Already in the first works on the analysis of a sharp increase in magnetostriction in $\text{Fe}_{100-x}\text{Ga}_x$ alloys in some ranges of x , the key factor for the occurrence of this effect was called the stabilization of the heterogeneous structure of the alloy. In the future, this assumption was the basis for the construction of numerous models. Indeed, with the help of microscopic research methods (HRTEM, XRD, SXRD, ND), many evidences of the specific organization of the alloy microstructure have been obtained. In some approximation, these testimonies can be divided into two groups. The first is the data on the bulk phase heterogeneity of the material, which manifests itself as the formation of nano-secrections (clusters) of an ordered phase in an unordered or less ordered matrix. The second group — evidence of the formation of non-standard tetragonal ordered phases for Fe-Ga, such as $m\text{-D0}_3$ (L6_0) or

D0_{22} . Numerous examples of both types of inhomogeneities are given in our recent reviews [4] and [5], the first of which mainly discusses the material properties of a wide range of iron-based alloys, and the second — structural studies of binary Fe-Ga- and Fe-Al-alloys.

It is not yet possible to come to a definite conclusion regarding the microscopic causes of the appearance of maxima in the dependences of magnetostriction on the content of Ga or Al, and further searches for correlations between the material characteristics and structural states of alloys are necessary. It is possible that the work on the triple system $\text{Fe}_{100-(x+y)}\text{Ga}_x\text{Al}_y$, which are currently practically absent, will allow us to advance in understanding the processes occurring in these alloys. For example, the analysis of the dependence of magnetostriction and damping ability of $\text{Fe}_{79.9}\text{Ga}_x\text{Al}_{20-x}\text{Tb}_{0.1}$ alloys (phase A2 with a short-range ordering of type D0_3) showed monotonous growth the magnitudes of saturation magnetostriction with increasing Ga content and the nonmonotonic dependence of the damping ability on the same factor [6].

This paper presents the results on the structural phase states of the compositions $\text{Fe}_{100-(x+y)}\text{Ga}_x\text{Al}_y$, with the total content of Ga and Al in 17, 26–28, 31 and 39 at.% obtained in neutron diffraction experiments. The analysis of neutronograms measured in the *in situ* mode with continuous heating to $\sim 900^\circ\text{C}$ and subsequent cooling to room temperature, and diffraction spectra measured with high resolution at a fixed temperature, made it possible to exhaustively characterize the structure and microstructure of alloys in the initial and final to obtain information about structural phase transitions occurring during their heating and cooling. The volumetric nature of the information obtained by neutron diffraction made it possible to exclude the effects associated with the surface layer (gallium evaporation), previously noted by us in the work [7], and local inhomogeneities of the structure [8].

2. Samples, experiment and data processing

In this paper, six compositions of $\text{Fe}_{100-(x+y)}\text{Ga}_x\text{Al}_y$ in the range of $17 \leq (x+y) \leq 39$ are investigated. Fe grades 008ZHR with purity of 99.99%, Ga with purity of 99.999% and Al with purity of 99.95% were used for the preparation of alloys. Before melting, the suspension was cleaned with ultrasound in an acetone medium. The melting was carried out in an induction vacuum furnace, the working space of which was evacuated, then it was filled with argon with a purity of 99.9995% to a pressure of 0.5 atm. After melting, the metal was aged 0.5 min, then gravity casting of the melt into a copper mold with an internal size of $60 \times 16 \times 4$ mm was carried out, which provided cooling at a high speed [9]. Samples in the form of parallelepipeds with dimensions of $4 \times 8 \times 50$ mm were cut out of the ingots. The specific compositions of the studied alloys and their initial phase states are presented in the table.

Compositions $\text{Fe}_{100-(x+y)}\text{Ga}_x\text{Al}_y$ for which neutron diffraction data were obtained. (The sample number corresponds to an increase in the total content of alloying elements $(x + y)$). The notation B2 + D0₃ means the cluster state of the microstructure (see section 3.1). The values of the parameters of the elementary cells are given for the cell α -Fe. The cubic cell of phase D0₃ has a 2 times larger parameter. The crystallographic characteristics of the phases discussed in this paper (A1, A2, B2, D0₃) are given in [5])

№	x	y	$x + y$	e/n	Phase	a , Å	V_a , Å ³
1	11.9	5.1	17.0	1.34	A2	2.9025	12.23
2	12.6	13.9	26.5	1.52	B2 + D0 ₃	2.9008	12.20
3	19.7	7.5	27.2	1.53	B2 + D0 ₃	2.9040	12.25
4	22.3	5.4	27.7	1.54	B2 + D0 ₃	2.9085	12.30
5	25.7	5.0	30.7	1.55	B2 + D0 ₃	2.9145	12.38
6	19.1	19.8	38.9	1.61	B2	2.9064	12.28

Measurements of neutron diffraction spectra were performed on a time-of-flight correlation diffractometer HRFD [10] (its detailed description is given in [11]) operating at the pulsed reactor IBR-2 at JINR (Joint Institute for Nuclear Research, Dubna city, Russia). For all samples in the initial cast state, high-resolution spectra were measured ($\Delta d/d \approx 0.0015$, measurement time 1 h). They were used to determine the phase state, analyze diffraction peak profiles, and accurately determine the unit cell parameter of samples. Examples of diffraction spectra measured with high resolution on two compositions are shown in Fig. 2. The compositions are in partially ordered phase states, and superstructural peaks resolved in the corresponding phases are present on the neutronograms. For phase B2 these are peaks with Miller indices $h + k + l \neq 2n$ (100, 111, etc.), for phase D0₃ these are peaks with Miller indices $h + k + l \neq 4n$ (111, 200 and etc.). The intensity of the superstructural peaks is relatively high, i.e. both the proportion of the sample volume occupied by the ordered phase and the degree of structure ordering are high. Superstructural peaks are absent in the disordered phase A2, i.e. at the transition D0₃ \rightarrow A2 only peaks with $h + k + l = 4n$ (220, 400, etc.) remain.

To obtain information about structural phase transitions occurring during heating and cooling of alloys, HRFD was switched to high-light intensity mode ($\Delta d/d \approx 0.015$, full spectrum measurement time 1 min). At the same time, the diffraction data set was carried out during continuous heating (up to $\sim 900^\circ\text{S}$) or cooling of the alloy with a temperature change rate of $\pm 2^\circ\text{C}/\text{min}$. The temperature calibration of the furnace was carried out according to the known temperature dependence of the parameter of the unit cell of silver, the ingot of which was heated and cooled in the furnace in an identical mode. The phase transformations occurring in the samples during heating and cooling can be conveniently traced by 2D maps of changes in the intensities of diffraction peaks (Fig. 3). By the disappearance of superstructural peaks during heating

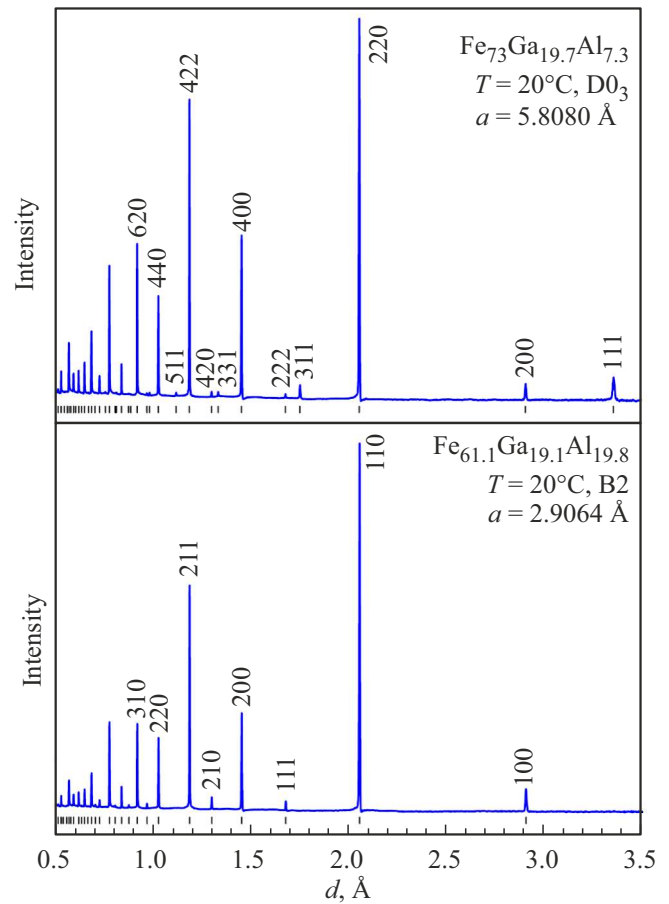


Figure 2. Neutron diffraction spectra of samples $\text{Fe}_{61.1}\text{Ga}_{19.1}\text{Al}_{19.8}$ (phase B2) and $\text{Fe}_{73.0}\text{Ga}_{19.7}\text{Al}_{7.3}$ (phase D0₃), measured in their original state. The calculated positions (vertical strokes) and Miller indices of the first peaks are shown.

and their appearance during cooling, the temperatures of transitions between phases with varying degrees of order are fixed. A changes in the volume fractions of structural phases and unit cell parameters are determined from the temperature dependences of the intensities and positions of the main peaks. The heating-cooling procedure was carried out with the compositions № 2, 4 and 5. With composition № 3, only heating was carried out. The spectra of compositions № 1 and 6 were measured only at room temperature.

In addition to the possibility of measuring diffraction spectra in high-resolution or aperture modes, another important feature of HRFD is that the functional dependence of the width of the diffraction peaks measured on it on the interplane distance is expressed by the simple formula $(\Delta d)^2 = C_1 + (C_2 + C_3)d^2 + C_4d^4$. Here C_1 and C_2 — some diffractometer constants determined in an experiment with a standard sample, C_3 takes into account the effect of microstresses in crystallites [$C_3 \approx (2\varepsilon)^2$], C_4 takes into account the effect of finite characteristic sizes of coherent scattering areas (CSA) [$C_4 \approx (k/L_{\text{coh}})^2$], k — a parameter

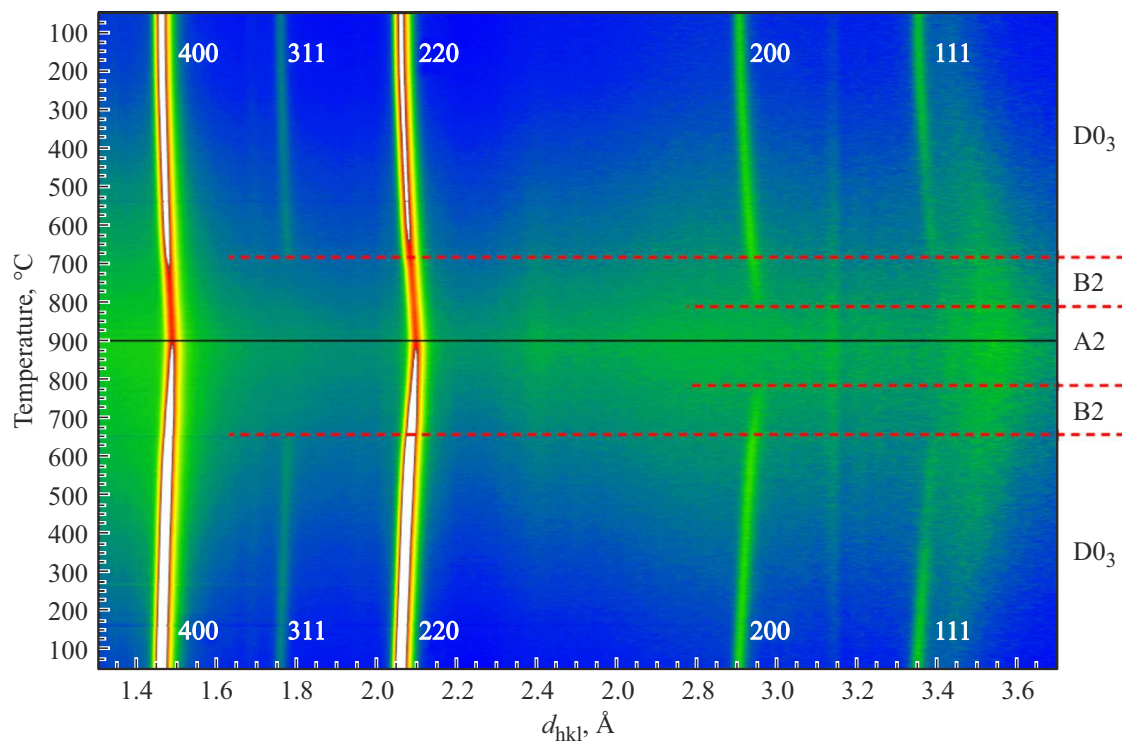


Figure 3. Diffraction spectra of the sample $\text{Fe}_{72.3}\text{Ga}_{22.3}\text{Al}_{5.4}$, measured during its continuous heating from 50 to 900°C and subsequent cooling to 50°C. The axis of temperature — from top to bottom, the axis of interplane distances — from left to right. Initial state — mixed B2 + D0₃ (conventionally denoted as D0₃), superstructural peaks 111, 200, 311 and main peaks 220 and 400 are indicated for it. When heated, transitions D0₃ → B2 occur (peaks 111 and 311 disappear), then B2 → A2 (peak 200 disappears). When cooling, the sequence of transitions is reversed. The 2D map contains 850 separate diffraction spectra.

that takes into account the shape of these areas and is close to unity in magnitude. In the absence of the size effect (large CSAs), the dependencies of $(\Delta d)^2$ on d^2 will be linear, if present — parabolic. Accordingly, by constructing these dependencies in a sufficiently large interval d_{hkl} , it is possible to determine ε (at the level of 0.001 and more) and L_{coh} (at the level of 3000 Å and less). The construction of such dependencies corresponds to the Williamson-Hall analysis (see, for example, [12]) adapted to the neutron time-of-flight method. The corresponding examples of the analysis of microstresses and sizes of CSAs in Fe-Ga and Fe-Al alloys are given in the review [5].

The analysis of diffraction data was carried out using the software package Fityk [13], with the help of which their main geometric characteristics were extracted from the description of the profile of bell-shaped functions: amplitude, area, position and width. The peak profiles were described by the Voigt function, which is a convolution of the Gaussian and Lorentzian. In this case, the full width of the peak at half height (FWHM) is some combination of the widths of the Gauss and Lorentz functions. Previously, in order to verify the processing method, clarify the diffractometer constants and its resolution function, the peak profiles of the standard powder La^{11}B_6 (neutron standard NIST) were analyzed.

3. Results

3.1. Heterogeneous (cluster) state of cast alloys

Traditionally, the phase state of an alloy is determined by the presence of certain basic and superstructural peaks in the diffraction spectra. Based on this criterion, in the initial state, the sample № 1 from the table with the minimum content of Ga and Al ($x + y = 17$) is in the disordered phase A2, the sample № 6 with the maximum content of these elements ($x + y = 39$) — in the partially ordered phase B2, the remaining samples — in the partially ordered phase D0₃. However, a more detailed examination, including an analysis of the widths and intensities of diffraction peaks, shows that the samples № 2–5 are in an inhomogeneous, B2 + D0₃, state. Indeed, as can be seen from Fig. 4, the experimental values of the peak widths of the composition $\text{Fe}_{72.3}\text{Ga}_{22.3}\text{Al}_{5.4}$, resolved in phase B2 (200, 220, etc.) and resolved in phase D0₃ (111, 311, etc.), lie on two different parabolic curves corresponding to markedly different characteristic sizes of coherent scattering areas. Similar dependencies were obtained for samples № 2–5. The states thus established for samples № 2–5 fully correspond to the cast structures for double Fe-Ga alloys, information about which is presented in [14].

Slow heating and subsequent cooling ($\pm 2^\circ\text{S}/\text{min}$) bring samples № 2–5 into a single-phase D0₃-state. This is

evidenced by Fig. 5, from which it can be seen that before heating, the experimental values of peak widths, as in Fig. 4, fall on two different parabolic curves. After cooling, all experimental points can be described by a

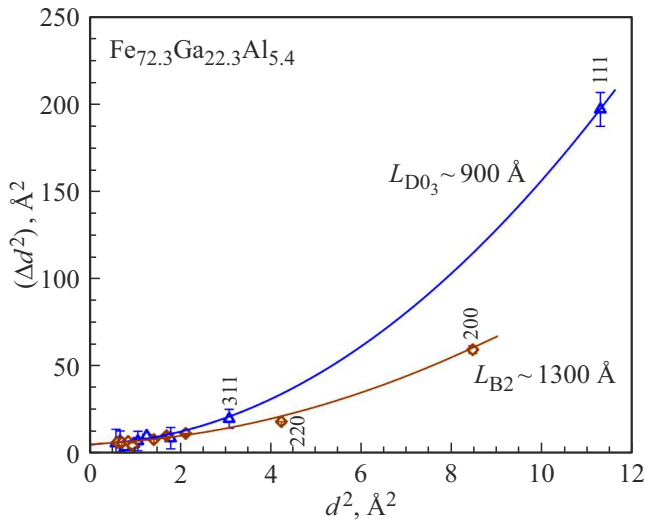


Figure 4. Williamson-Hall constructions for the width of diffraction peaks of the composition $\text{Fe}_{72.3}\text{Ga}_{22.3}\text{Al}_{5.4}$ in the cast state. The characteristic sizes of the CSAs for the matrix B2 and clusters D_{03} are indicated. Miller indices of points are given for phase D_{03} , the values of Δd are multiplied by 10^3 . The errors of most points are close to the size of the characters.

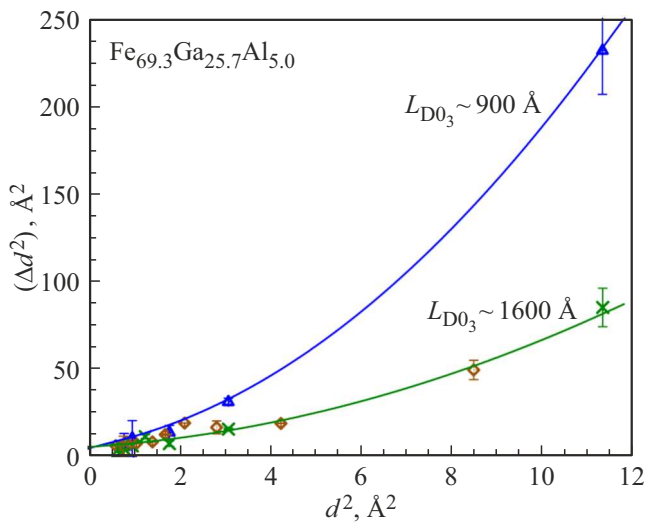


Figure 5. Williamson-Hall constructions for the width of diffraction peaks of the composition $\text{Fe}_{69.3}\text{Ga}_{25.7}\text{Al}_{5.0}$ in the cast state. For the initial cast state, the experimental points fall into two different dependencies: for the matrix B2 (rhombuses, peaks 200, 220, etc.) and for clusters D_{03} (triangles, peaks 111, 311, etc.). After cooling, the experimental points (crosses) fall on a single curve. The characteristic sizes of the CSAs clusters D_{03} before heating (900 Å) and the homogeneous phase D_{03} after cooling are indicated. Miller indices of points are given for phase D_{03} , the values of Δd are multiplied by 10^3 . The errors of many points are close to the size of the characters.

single dependence, i.e. a homogeneous phase D_{03} was formed. The new dependence corresponds well to the curve that described the peak widths from the matrix B2 before heating.

The combination B2/ D_{03} , as the structural state of the matrix and clusters, was also observed in double alloys Fe-Ga and Fe-Al [3,5]. It was also found that, depending on the background (method of preparation, temperature exposure, etc.), other combinations of structural phases acting as matrices and clusters (A2/B2, A2/ D_{03}) are possible in these alloys.

3.2. Phase transitions with temperature change

The phase transformations occurring in the samples during heating and cooling are well traced by 2D maps of changes in the intensities of diffraction peaks (Fig. 3). Transition temperatures can be estimated by the disappearance and appearance of superstructural peaks. They are determined more precisely from the temperature dependences of their integral intensities, which for one of the samples are shown in Figs. 6 and 7 (heating and cooling). When heated, the mixed state (matrix B2 + clusters D_{03}) exists up to $T \approx 640^\circ\text{C}$, above which the alloy passes into a partially ordered phase B2, and above $T \approx 715^\circ\text{C}$ to the disordered phase A2. When cooling from 900°C , the states change in reverse order, the transition temperature $\text{A2} \rightarrow \text{B2}$ does not change ($T \approx 715^\circ\text{C}$), and the transition temperature to the homogeneous phase D_{03} drops slightly ($T \approx 630^\circ\text{C}$). Such a sequence of transitions is observed in the compositions № 2, 3 and 4.

A feature of the composition № 5 is the formation of the A1 phase upon heating, the diffraction peaks of which are visible in the spectra in the temperature range ($440\text{--}700^\circ\text{C}$) (fig. 8). The volume fraction of this phase does not exceed 10%, however, synchronously with its appearance there is a noticeable increase in the width of the peaks of the main phase shown in this figure, which is associated with the occurrence of strong microstresses in the crystallites. As follows from our X-ray diffraction data, with prolonged annealing of this sample (300 h at 450°C), the A1 phase becomes the main one.

From Figs. 6 and 7 for the composition of $\text{Fe}_{73.5}\text{Ga}_{12.6}\text{Al}_{13.9}$ it can be seen that in the area of transitions $\text{B2} \leftrightarrow \text{B2} + \text{D}_{03}$ deviations from the linear behavior of the dependence of the atomic volume on temperature, $V_{as}(T)$, are observed, and they clearly correlate with the appearance or disappearance of the superstructural peak 311 of phase D_{03} . This effect has the same nature as the dependence of V_a on $(x + y)$ shown in Fig. 1, the transition to a more ordered state leads to a reduction in the parameters of the unit cell and vice versa. Similar effects were observed for binary Fe-Ga [3], Fe-Al [15] and triple Fe-Al-Cr [16] alloys. Outside the transition area $\text{B2} \leftrightarrow \text{B2} + \text{D}_{03}$, the change of V_a with temperature is linear, and the coefficients of thermal expansion or compression are almost the same, $\beta = (\Delta V/V)/\Delta T \approx \pm 8 \cdot 10^{-5} \text{K}^{-1}$, which

is about 2 times more than cast iron. During the transition, the relative volume change is about $3.3 \cdot 10^{-3}$,

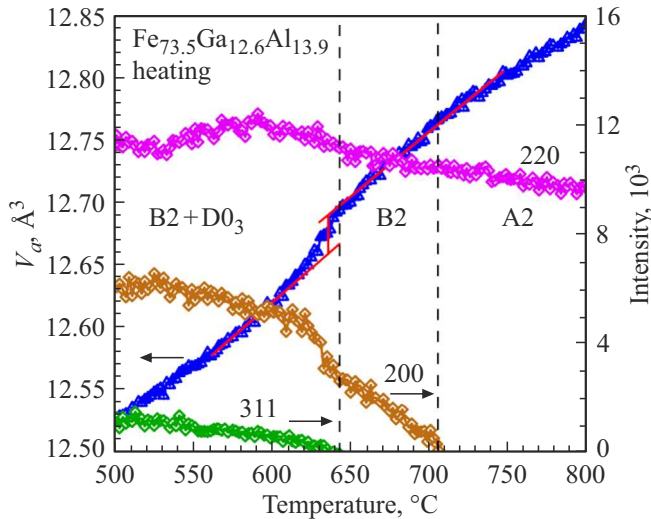


Figure 6. Dependences on the temperature of the atomic volume (left scale) and the intensities (right scale) of characteristic diffraction peaks (Miller indices are indicated for the phase D₀₃) for the composition Fe_{73.5}Ga_{12.6}Al_{13.9} when it is heated. The vertical lines indicate the transition temperatures B2 + D₀₃ → B2 (the superstructural peak disappears 311) and B2 → A2 (the superstructural peak disappears 200). The main peak of 220 exists in all states. Inclined lines — description of the behavior of the atomic volume by a linear function in the temperature ranges before and after the transition from the mixed state to the B2 phase. A conditional jump of volume is shown.

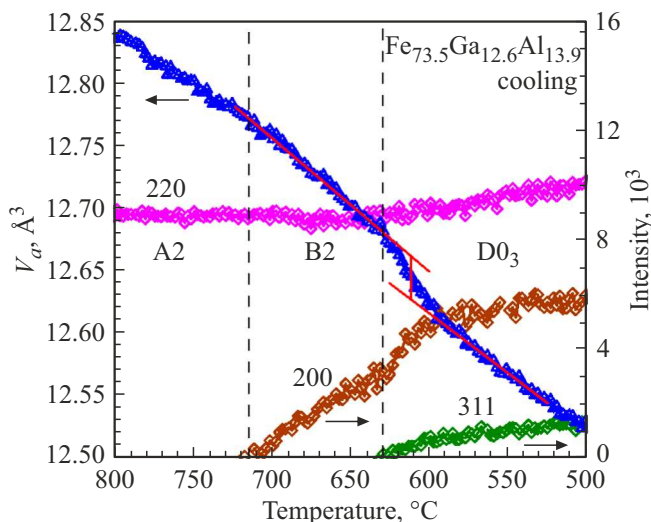


Figure 7. The same as in Fig. 6, but for cooling. The vertical lines indicate the transition temperatures A2 → B2 (a superstructural peak 200 appears) and B2 → D₀₃ (a superstructural peak 311 appears). The main peak of 220 exists in all states. Inclined lines — description of the behavior of the atomic volume by a linear function in the temperature intervals before and after the temperature of the occurrence of the ordered phase D₀₃. A conditional jump of volume is shown.

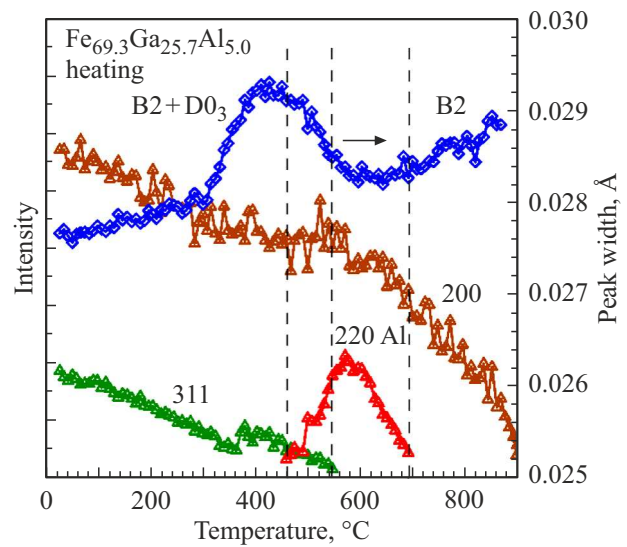


Figure 8. Temperature dependences of the intensities (right scale) of the superstructural diffraction peaks 200 and 311 of phase D₀₃ and peak 200 of phase A1 for the Fe_{73.5}Ga_{12.6}Al_{13.9} with its heating. The width of the main peak 400 is indicated by diamonds (left scale). The vertical lines indicate the transition temperatures A1 + B₂₃ → D₀ (the superstructural peak disappears 311) and B₂ → A₂ (the superstructural peak disappears 311). Phase B₂ exists up to 900°S.

which corresponds to a change in the cell parameter $\Delta a/a = (\Delta V/V)/3 \approx 1.1 \cdot 10^{-3}$. Similar values of the „jump“ parameter (volume) were obtained for samples № 3–5. The temperature interval of the transition from one linear dependence to another is $\Delta T \approx .30^\circ\text{S}$, which indicates its delayed kinetics. At the same time, the processes of decreasing (increasing) the fraction of the sample volume occupied by the ordered phase and the degree of order in it occur. In the dependences of the intensities of superstructural peaks on temperature, these processes do not manifest themselves explicitly. Figures 6 and 7 show, in addition, that the transitions A₂ ↔ B₂ have almost no effect on the linear change of the parameter with temperature, only slightly changes the slope of the dependence, namely, it becomes about $30T > 720^\circ\text{C}$.

3.3. Coherence of elementary matrix cells and clusters

Possible reasons for the effect of a certain decrease in the cubic lattice parameter during the transitions of Fe-Ga and Fe-Al alloys from a less ordered to a more ordered state are discussed in the review [5]. From the data obtained, (presented in Fig. 1, 6, 7) it follows that this effect is also manifested in the triple alloy Fe-Ga-Al, since the deviation from the linear dependence occurs during the formation of phases D₀₃ or B₂ from phase A₂. In the case of the cluster state of the microstructure, the effect of parameter reduction should manifest itself in the distortion of the profiles of the

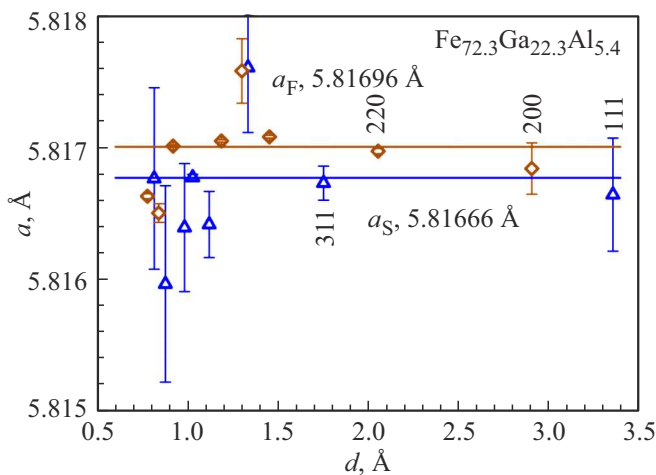


Figure 9. Parameters of elementary matrix cells (rhombuses, a_F) and clusters (triangles, a_S) for the composition $\text{Fe}_{72.3}\text{Ga}_{22.3}\text{Al}_{5.4}$, determined from the positions of individual (fundamental and superstructural) diffraction peaks. Miller indices of points are given for phase D0_3 . For the matrix (phase B2), the parameter value is doubled. Statistical errors of points are indicated.

main diffraction peaks in high-resolution spectra. Indeed, in this case, the diffraction peaks should be the sum of the peaks from the matrix and from the clusters shifted relative to each other by $\Delta a/a \approx 1 \cdot 10^{-3}$ ($\Delta d \approx 0.002 \text{ \AA}$ for a peak of 400), that it should lead to asymmetry of profiles or even to splitting of peaks. However, a specially conducted analysis showed (for Fe-Ga, this was done in [3]) that the profiles of the main peaks actually repeat the profiles of peaks from the standard polycrystal LaB_6 , which are determined by the resolution function of the diffractometer, i.e. the expected difference in the parameters of the matrix and cluster cells, it does not introduce any noticeable broadening and shift. This means that a very high degree of coherence is maintained between the crystal lattices of the matrix and clusters and the parameters of their cells must coincide or be close to each other.

For the first time this assumption was formulated and verified in [17]. For verification, the positions of diffraction peaks in the d_{hkl} scale were determined and then the values of the cell parameter were calculated individually for each peak. The matrix cell parameter was determined from the positions of the main peaks, and the cluster cell parameter was determined from the positions of the superstructural peaks. It has been shown that these parameters coincide with each other with accuracy better than $\Delta a/a = 1 \cdot 10^{-4}$ (up to $\Delta a/a \approx 1 \cdot 10^{-5}$), which is at least 10 times less than the parameter change during ordering.

For samples of Fe-Ga-Al in a mixed B2 + D0_3 -state, it is possible to process profiles of (8–9) peaks from the matrix with acceptable accuracy and (5–6) peaks from clusters. A typical example of the corresponding analysis is shown in Fig. 9. It follows from it that the possible relative difference between the parameters of matrix cells B2 and clusters

D0_3 is about $5 \cdot 10^{-5}$ ($\Delta a \approx 0.0003 \text{ \AA}$). This value is about 20 times less than the observed parameter changes during transitions $\text{B2} + \text{D0}_3 \leftrightarrow \text{B2}$, shown in Figs. 6 and 7, and about 70 times less, than the value following from *ab initio* calculations performed in [18] for transitions $\text{B2} \leftrightarrow \text{D0}_3$ in compositions Fe-Ga.

4. Discussion and conclusion

As noted in the Introduction, to compare the structural properties of double $\text{Fe}_{100-x}\text{Ga}_x$, $\text{Fe}_{100-y}\text{Al}_y$ and triple $\text{Fe}_{100-(x+y)}\text{Ga}_x\text{Al}_y$ alloys as a parameter, you can use the value of $(x+y)$ — their total presence in the alloy. The reason for this is that for Ga and Al, the number of free electrons is assumed to be the same ($e = 3$) and the values e/n (the ratio of the number of free electrons to the number of atoms) and $(x+y)$ can be used equally. If this is the case, then the neutron diffraction data obtained in this work indicate that the structural properties of these three types of alloys are largely identical, although there are some differences.

The structural phase diagrams (both equilibrium and metastable) of double alloys are well known and described in detail (see, for example, [19,20,4,14]) and, nevertheless, continue to be refined [21]. In Fe-Al alloys up to 50 at.% Al, no other phases except A2, D0_3 and B2 were detected [15], including when they were heated right up to melting. In cast compositions $\text{Fe}_{100-x}\text{Ga}_x$ up to $x \approx 30$, the situation is the same, but at $x > 30$, $\text{Fe}_{13}\text{Ga}_9$ intermetallide with a monoclinic structure [22] begin to form in them. Slow heating of the compositions $\text{Fe}_{100-x}\text{Ga}_x$ with $x > 24$ leads to the appearance of phases L1_2 and D0_{19} , derived from A1 and A3-structures, and for $x > 32$, there is also a monoclinic phase $\alpha\text{-Fe}_6\text{Ga}_5$. For example, a detailed analysis of the structural transformations of the compositions $\text{Fe}_{100-x}\text{Ga}_x$ at $x \approx 26$ (in terms of the content of Ga, an analogue of the sample № 5), performed in [23], showed that in the original cast the samples are in a homogeneous phase D0_3 , which, when heated, is first transformed into L1_2 (at 450°C), then into D0_{19} (at 600°C), above 700°C — in the disordered phase A2. When cooling, the situation depends on the content of Ga, at $x \approx 25$, the main phase becomes L1_2 , and at $x \approx 27$, a mixed state $\text{L1}_2 + \text{D0}_{19}$ occurs.

From the data given in this paper for ternary alloys, it follows that up to $(x+y) \leq 31$ only A2, D0_3 and B2-phases are observed in them, including when heated to $\sim 900^\circ\text{C}$ and subsequent cooling. Only when the composition is heated with $(x+y) = 30.7$ in the temperature range $(450\text{--}700)^\circ\text{C}$ with the phase A1 appeared in a small amount. No signs of monoclinic phases were found. It can be concluded that in the nonequilibrium (as-cast) state at room temperature, triple alloys $\text{Fe}_{100-(x+y)}\text{Ga}_x\text{Al}_y$ by their structural properties up to $(x+y) \approx 39$ repeat $\text{Fe}_{100-y}\text{Al}_y$ alloys in the same range of Al content. Comparison of phase diagrams of Fe-Ga and Fe-Al alloys in the concentration range up to 35 at.% was spent in [24]. In this paper

it is noted that in general the structure of the diagrams is the same and in fact the only noticeable difference is that $(D0_3)$ -Fe₃Ga-the phase exists up to temperatures at $\sim 100^\circ$ With higher than $(D0_3)$ -Fe₃Al. It follows from our data that in ternary compositions, the temperature range of the existence of a phase with the structure $D0_3$ has some similarity with Fe-Ga alloys, and the transitions $B2 \rightarrow A2$ are shifted lower in temperature in comparison with Fe-Ga, and with Fe-Al-compositions.

The initial cluster state of the samples № 2–5 is typical for double alloys Fe_{100-x}Ga_x with $19 \leq x \leq 24$ and Fe_{100-y}Al_y with $20 \leq y \leq 30$ [3]. As the model calculations show, and the experiment confirms, in the process of ordering the structure, areas with a near and then with a far order appear, dispersed in an unordered matrix. Such a cluster microstructure can be fixed during various thermal effects on the alloy. As a limiting case of a cluster microstructure, antiphase domains (APD) are formed in the entire volume of the material during prolonged thermal exposure. In triple alloys, the cluster state is observed up to $(x + y) \approx 31$. This is noticeably more than for Fe_{100-x}Ga_x, and in about the same range as for Fe_{100-y}Al_y, although in samples № 3–5 the content of Ga is 3–5 times greater than the content of Al. Some difference from double alloys is that the characteristic sizes of CSAs in clusters (which can be considered a lower estimate of cluster sizes) in the initial cast state are close to 1000 Å, whereas in Fe-Ga and Fe-Al alloys they are as a rule, they do not exceed several hundred Å. This characteristic, however, is not strictly defined and may depend on the cooling rate of the alloy.

Diffraction measurements with high resolution made it possible to independently determine the values of the parameters of the elementary cells of the matrix and clusters. As in the case of double alloys, it turned out that the difference between them, if there is, is very small ($\Delta a \approx 0.0003$ Å or less). This means that a high degree of coherence is maintained between the matrix (phase B2) and the clusters (phase $D0_3$). The analysis of the temperature dependences of the cell parameters showed that in the initial state their values correspond to an ordered state, i.e. the matrix adapts to clusters, despite the fact that its volume fraction is obviously larger than that of clusters.

Summarizing, we can say that the structural properties of cast alloys Fe_{100-(x+y)}Ga_xAl_y up to $(x + y) \approx 40$ basically repeat the properties of the double compositions Fe_{100-x}Ga_x up to $x \approx 30$ and Fe_{100-y}Al_y up to $y \approx 50$, and the observed differences It can be logically explained by the partial replacement of Ga atoms with Al atoms. For example, the expansion of the range of formation of cubic phases based on the BCC cell in ternary alloys in comparison with Fe_{100-x}Ga_x indicates the role of Al in the stabilization of these states. In addition, the addition of a relatively small amount of Al (5%) in the composition of Fe-26Ga leads to suppression of the formation of the equilibrium (for the Fe-Ga system) L1₂-phase.

Funding

Neutron diffraction experiments were performed on a neutron source IBR-2 (JINR, Dubna city, Russia). This work was supported financially by RSF (project No. 22-42-04404).

Conflict of interest

The authors declare that they have no conflict of interest.

References

- [1] E.M. Summers, T.A. Lograsso, M. Wun-Fogle. *J. Mater. Sci.* **42**, 9582 (2007).
- [2] J.B. Restorff, M. Wun-Fogle, K.B. Hathaway, A.E. Clark, T.A. Lograsso, G. Petculescu. *J. Appl. Phys.* **111**, 023905 (2012).
- [3] A.M. Balagurov, I.A. Bobrikov, S.V. Sumnikov, I.S. Golovin. *J. Alloys Compd.* **895**, 162540 (2021).
- [4] I.S. Golovin, V.V. Palacheva, A.K. Mohamed, A.M. Balagurov. *FMM* **121**, 937 (2020).
- [5] A.M. Balagurov, I.S. Golovin. *UFN* **191**, 738 (2021).
- [6] H.W. Chang, S.U. Jen, Y.H. Liao, F.C. Chang, W.C. Chang, J. Cifre, D.G. Chubov, I.S. Golovin. *J. Alloys Compd.* (2022). Submitted.
- [7] T.N. Verzhinina, I.A. Bobrikov, S.V. Sumnikov, A.O. Boev, A.M. Balagurov, A.K. Mohamed, I.S. Golovin. *Intermetallics* **131**, 107110 (2021).
- [8] I.A. Bobrikov, N.Y. Samoylova, S.V. Sumnikov, O.Y. Ivanshina, E.K. Korneeva, A.M. Balagurov, I.S. Golovin. *J. Appl. Cryst.* **53**, 1343 (2020).
- [9] I.S. Golovin, A.M. Balagurov, I.A. Bobrikov, S.V. Sumnikov, A.K. Mohamed. *Intermetallics* **114**, 106610 (2019).
- [10] A.M. Balagurov. *Neutron News* **16**, 8 (2005).
- [11] A.M. Balagurov, I.A. Bobrikov, G.D. Bokuchava, V.V. Zhuravlev, V.G. Simkin. *Physika elementarnykh chastits i atomnogo yadra* **46**, 453 (2015).
- [12] E.J. Mittemeijer, U. Welzel. *Z. Kristallogr.* **223**, 552 (2008).
- [13] M. Wojdyr. *J. Appl. Cryst.* **43**, 1126 (2010).
- [14] I.S. Golovin, A.M. Balagurov, I.A. Bobrikov, S.V. Sumnikov, A.K. Mohamed. *Intermetallics* **114**, 106610 (2019).
- [15] A.M. Balagurov, I.A. Bobrikov, I.S. Golovin. *Pis'ma v ZhETF (in Russian)*. **110**, 584 (2019).
- [16] A.M. Balagurov, I.A. Bobrikov, S.V. Sumnikov, I.S. Golovin. *Phys. Rev. Materials* **3**, 013608 (2019).
- [17] A.M. Balagurov, I.A. Bobrikov, B. Mukhametuly, S.V. Sumnikov, I.S. Golovin. *Pis'ma v ZhETF* **104**, 560 (2016).
- [18] M.V. Matyunina, M.A. Zagrebin, V.V. Sokolovskiy, O.O. Pavluchina, V.D. Buchelnikov, A.M. Balagurov, I.S. Golovin. *Phase Transitions* **92**, 101 (2019).
- [19] O. Kubaschewski. *Iron — Binary phase diagrams*. Springer-Verlag (1982).
- [20] H. Okamoto. *Bull. Alloy Phase Diagrams* **11**, 576 (1990).
- [21] A.K. Mohamed, V.V. Palacheva, V.V. Cheverikin, T.N. Verzhinina, A.M. Balagurov, G.M. Muralikrishna, N. Esakkiraja, S.V. Divinski, G. Wilde, I.S. Golovin. *Intermetallics* **145**, 107540 (2022).
- [22] I.S. Golovin, V.V. Palacheva, A.K. Mohamed, J. Cifre, L.Yu. Dubov, N.Yu. Samoylova, A.M. Balagurov. *J. Alloys Compd.* **874**, 158882 (2021).

- [23] I.S. Golovin, A.K. Mohamed, V.V. Palacheva, V.V. Cheverikin, A.V. Pozdnyakov, V.V. Korovushkin, A.M. Balagurov, I.A. Bobrikov, N. Fazel, M. Mouas, J.-G. Gasser, F. Gasser, P. Tabary, Q. Lan, A. Kovacs, S. Ostendorp, R. Hubek, S. Divinski, G. Wilde. *J. Alloys Compd.* **811**, 152030 (2019).
- [24] O. Ikeda, R. Kainuma, I. Ohnuma, K. Fukamichi, K. Ishida. *J. Alloys Compd.* **347**, 198 (2002).